Modal Behaviour Assessment Using IGA on Automotive NVH Analysis

Felipe Vieira[1], Lluis Martorell[1], Ovidi Casals[1], Angélica Sánchez[1]

Courtesy of: Xabier Larrayoz[2]

[1]Applus+ IDIADA
L'Albornar – PO Box 20, 43710 Santa Oliva, Spain

[2]SEAT-CUPRA
Autovía A-2, km. 585, 08760 Martorell, Spain

1 Motivation

The interest of the automotive industry in Isogeometric Analysis (IGA) [1] technology is growing each year. The goal is to integrate the technology into current workflows, which generally means initially looking for options implemented in commercial software already being used. This makes the framework using ANSA as pre-processor, to generate the IGA models, and LS-DYNA as the solver very appealing as both are already present in the automotive environment. Because LS-DYNA is used mainly in crashworthiness, all presentations of IGA in automotive industrial conferences have focused until now on crash applications [2, 3]. However, the academic literature shows how IGA behaves with greater accuracy and robustness in general compared to Finite Element Analysis (FEA) with less degrees of freedom and for time dependent problems how you get superior discrete spectrum [4]. In the explicit setting this allows for larger time steps compared to FEA and in the implicit setting it improves the conditioning of linear systems compared to FEA. To the authors knowledge no industrial assessment have been done yet using LS-DYNA implicit solver and its IGA capabilities for Noise, Vibration , and Harshness (NVH) or Stiffness applications. This work aims to evaluate the current status of the LS-DYNA's IGA implicit implementation for NVH analysis and compare against established FEA procedures currently employed in automotive NVH teams. The goal is to check its viability to perform full vehicle simulations using IGA and identify early problems that need to be addressed.

2 Introduction

Modal analysis is the study of the dynamic properties of systems in the frequency domain. The governing equation for undamped free vibration of a structural system can be expressed as:

$$\boldsymbol{M}\ddot{\mathrm{u}}(t) + \boldsymbol{K}\boldsymbol{u}(t) = 0$$

where $\boldsymbol{M}$ represents the mass matrix, $\boldsymbol{K}$ denotes the stiffness matrix, and $\boldsymbol{u}$ indicates the displacement vector. Assuming solutions of the form $\boldsymbol{u}(t) = \boldsymbol{\psi}\mathrm{e}^{\mathrm{i}\omega\mathrm{t}}$, where $\boldsymbol{\psi}$ is the mode shape vector, ω is the natural frequency and $i = \sqrt{-1}$, the governing equation is reduced to an eigenvalue problem:

$$(\boldsymbol{K} - \omega^2\boldsymbol{M})\boldsymbol{\psi} = 0$$

The eigenvalues ω^2 yield the natural frequencies of the system, and the eigenvectors $\boldsymbol{\psi}$ describe the shapes associated with the mode. The total structural response to an external excitation is often expressed as a superposition of modal contributions. The modal expansion principle allows the dynamic response, under arbitrary loading conditions, to be reconstructed by summing the contributions of each mode. This methodology is particularly powerful in the frequency domain where Frequency Response Functions (FRFs) can be constructed and analysed. For a more in-depth explanation of the governing equations for mechanical vibrations, including the analytical dynamics of discrete systems, the analysis of undamped and damped vibrations of n-degree-of-freedom systems with their eigenmodes and eigenfrequencies, and associated computational methods, the reader is encouraged to consult the book of Geradin and Rixen [5]

To understand the theory behind IGA, the reader is directed to the PhD work of Leidinger [6] where an in depth explanation of IGA is done.

2.1 Formentor CUPRA base model

As an initial assessment, modal analysis simulations are performed to compare benchmark models of increasing complexity. Some of this benchmark models are based on the design models used for the compact crossover Sport Utility Vehicle (SUV) Cupra Formentor from the Spanish car manufacturer SEAT under their Cupra sub-brand. The models are of the original version, before the facelift of 2022. SEAT allowed for the geometry and results to be shown, but not the frequency values of the modes. Therefore, all comparisons shown in this work are relative errors compared to the original NASTRAN-FEA version of the model, but no absolute values are provided.

For a general perspective, a good margin for a correlation activity in automotive applications between experimental data and simulation results must be, at least, below the 5% difference in frequency value. As the absolute frequency value cannot be shown in this document, when showing frequency results in the following benchmarks, the plotted value in graphs will be the relative percentage differences compared to the NASTRAN model, according to the formula:

$$\Delta\,\omega_{\mathrm{i}} = \frac{\left(\omega_{\mathrm{i}} - \omega_{NASTRAN,i}\right)}{\left(\omega_{\mathrm{NASTRAN,i}}\right)}\ \mathrm{x}\ 100$$

where ω_i is the frequency of the mode i of the model being analysed and $\omega_{NASTRAN,i}$ is the frequency for the same mode calculated using NASTRAN. Therefore, negative values will indicate that the model is less stiff than the NASTRAN version and positive values that the model is stiffer than the NASTRAN version. Moreover, for industrial validation, the Modal Assurance Criterion (MAC) serves as the standard metric to quantify the correlation of the mode shape between different models or between simulation and experimental results. The formula for the MAC of two modes i and j is a normalized inner product between the two eigenvectors:

$$MAC_{ij} = \frac{\left|\boldsymbol{\Psi}_i^T \cdot \boldsymbol{\Psi}_j\right|^2}{\left(\boldsymbol{\Psi}_i^T \cdot \boldsymbol{\Psi}_i\right)\left(\boldsymbol{\Psi}_j^T \cdot \boldsymbol{\Psi}_j\right)}$$

where $\boldsymbol{\Psi}_{\mathrm{i}}$ and $\boldsymbol{\Psi}_{\mathrm{j}}$ are the eigenvectors for the modes i and j, and "$\cdot$" represents the inner product. MAC values range from 0 to 1, with values greater than 0.95 typically indicating good correlation and values greater than 0.9 considered acceptable for industrial applications.

2.2 NASTRAN to LS-DYNA conversion

The starting point for the analysis of the BiW performed in this project was a NASTRAN FEA model of the CUPRA-Formentor. Since NASTRAN is a de-facto industry standard for modal analysis and other NVH applications, it was first necessary to verify that a sufficiently accurate equivalency between NASTRAN-FEA and LS-DYNA-FEA models could be obtained at coupon, component and full-vehicle levels. Once this is demonstrated, further comparison between LS-DYNA FEA and IGA is possible. The connections to other components, controls and general assembly will be the same. *Table 1*: *Equivalence table of NASTRAN objects to LS-DYNA definitions. Based on [7–10] and IDIADA internal experience.* summarizes the translation of NASTRAN objects present in the models used to represent them in LS-DYNA. Some of the reference material to create this table is in the table caption for the reader to check if needed.

Table 1: *Equivalence table of NASTRAN objects to LS-DYNA definitions. Based on [7–10] and IDIADA internal experience.*

	NASTRAN	LS-DYNA
1D elements	CBUSH	***SECTION_BEAM** with ELFORM=6 + ***MAT_66**
	RBAR/RBE2	***CONSTRAINED_NODAL_RIGID_BODY**
	RBE3	***CONSTRAINED_INTERPOLATION**
Spotweld	CWELD	ACM2 (hexahedral element with RBE3 ties)
Shell elements	CQUAD4	***SECTION_SHELL** with ELFORM=20
Solid elements	CHEXA8 / CPENTA6	***SECTION_SOLID** with ELFORM=18
	CTETRA10	***SECTION_SOLID** with ELFORM=16
Materials	MAT1	***MAT_ELASTIC** (MAT_001)

With respect to the materials, all materials are linear and isotropic. However, MAT1 from NASTRAN allows to define the material properties with the Shear Modulus, G, but *MAT_ELASTIC from LS-DYNA

must be defined only with the Young modulus, E and the Poisson ratio ν. As the materials are isotropic, the following relation can be used to translate the materials to LS-DYNA:

$$E = 2G(1+\nu)$$

With respect to spotwelds, CWELD is a coarse spotweld model, implemented in NASTRAN as a special shear flexible beam type element with two nodes and twelve degrees of freedom, primarily used to model large spotwelded structures such as automotive Body in White (BiW). It allows three different configurations to connect a surface to a surface, an element to an element, or a point to an element as seen in *Figure 1*. The alternative to the CWELD is the ACM2 spotweld configuration, which consist of defining an hexahedral element connecting surfaces via RBE3 connections.

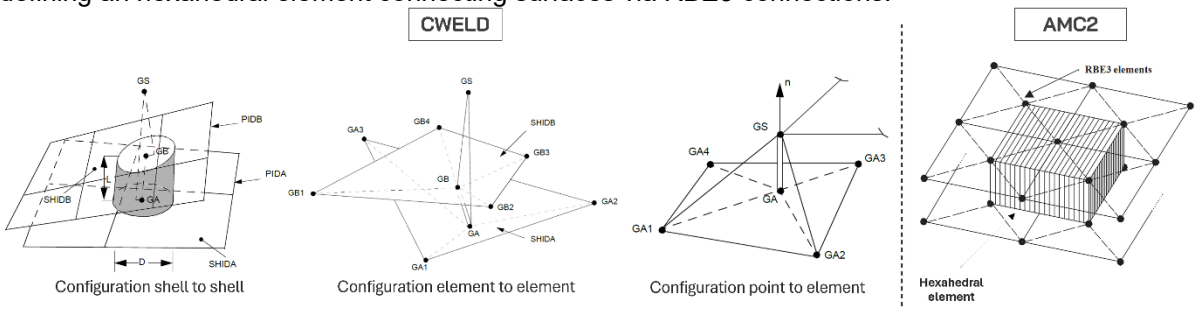

Figure 1: CWELD and AMC2 spotweld configurations. Image adapted from [11-12]

This means that the ACM2 configuration for the spotwelds needs to be updated in the original Formentor CAE model before the IGA introduction. The transformation is done using the ANSA Connection Assembly tool. *Figure 2* shows some regions of the BiW with the new spotweld configuration.

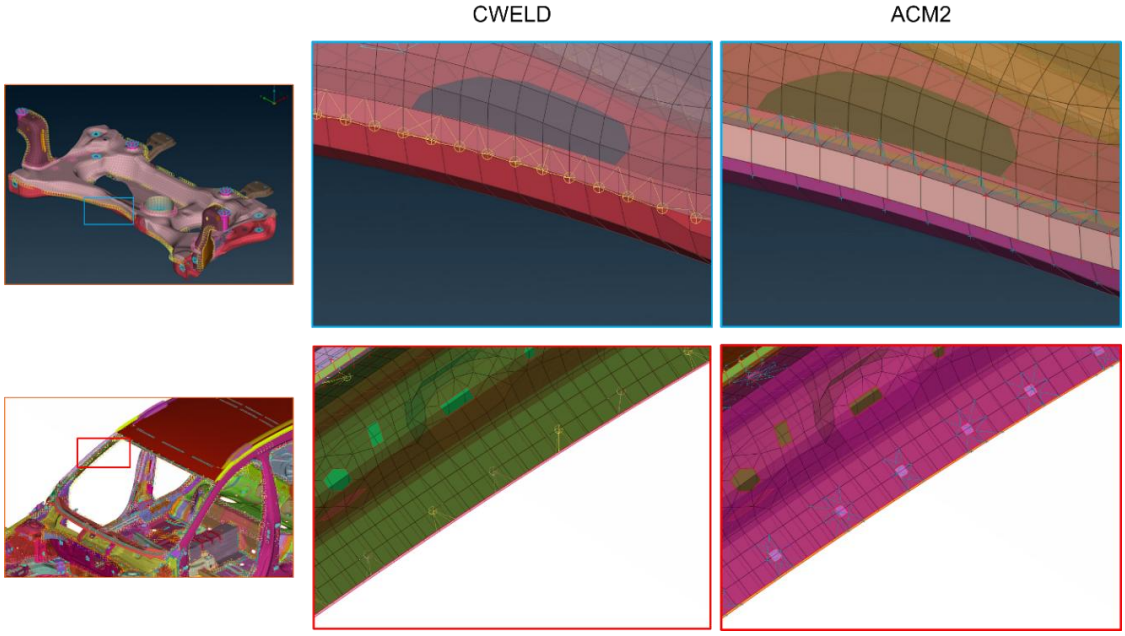

Figure 2: Conversion of CWELDs configuration to its ACM2 equivalent using the Connection Assembly tool from ANSA pre-processor.

3 IGA shell modal analysis assessment

For IGA shells three benchmark problems analysed are: a square plate, the B-pillar of the Formentor vehicle, and the BiW also of the Formentor. This allows to fix parameters for the more complex benchmarks in the first ones or to check the results for the more complex cases are coherent with previous results.

3.1 Plate benchmark

This first benchmark goal is to perform a controlled comparison of the element formulation to be used for IGA. A flat rectangular plate of 100mm x 100mm is defined with a thickness of 2mm. Stainless steel material properties are assigned with Young's modulus $E = 200000\ MPa$, Poisson's ratio $\nu = 0.3$ and density $\rho = 7.85E-9\frac{T}{mm^3}$. The boundary conditions on the edges are Free-Free. The FEA

discretizations is made using 5mm elements and using ELFORM=20, corresponding to the fully integrated linear assumed strain C0 shell. The IGA discretization employed was created with ANSA, using a quadratic degree, a uniform knot vector, not activating the extend function, an average knot span of 5mm, and ELFORM=3, which corresponds to a Reissner-Mindlin element. For all the results shown in this work, the keyword **`*CONTROL_IMPLICIT_CONSISTENT_MASS`** is used. *Figure 3* shows a comparison of the frequency values for the first 9 modes of the plate. LS-DYNA-FEA model shows less than 0.5% relative error compared to the NASTRAN results. And the IGA model shows a higher difference, but below the 2.5%, which can be considered acceptable. The IGA behaviour is less stiff compared to FEA results. The results of a non-trimmed IGA version of the plate are also displayed, showing similar results to the trimmed version. This comparison shows that the use of trimmed models does not negatively affect compared to untrimmed models. However, for more complex geometries, ANSA is only able to generate trimmed geometries.

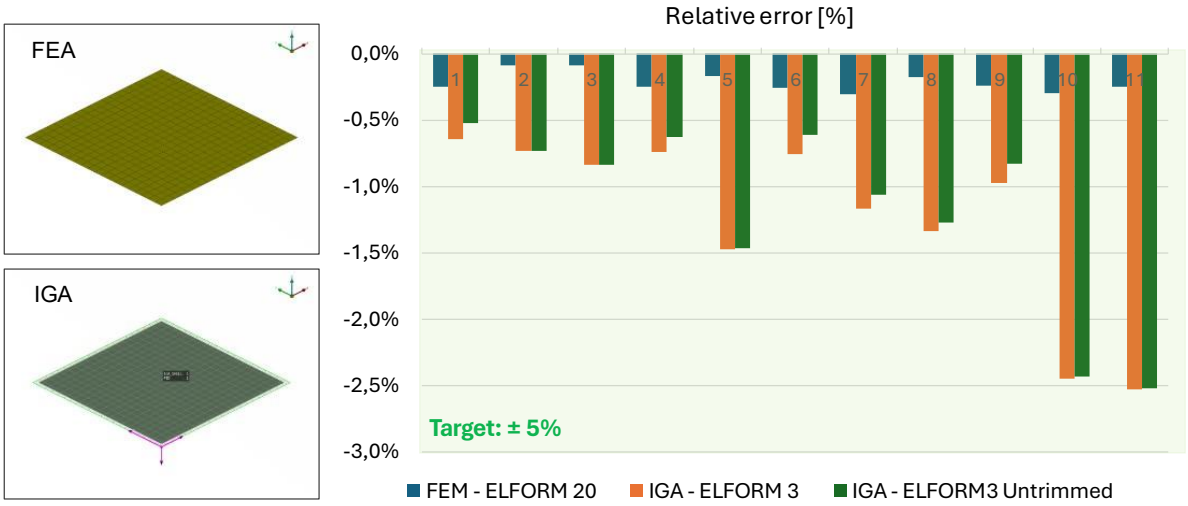

Figure 3: Relative comparison of the frequencies of the first nine modes of the plates between the NASTRAN simulation and the LS-DYNA simulations.

Figure 4 shows the effect of increasing the degree of the IGA surface. For this plate with free-free boundary conditions, increasing the degree of the surface and maintaining the knot span size, 5mm, does not provide an improvement in the results. For the rest of the benchmarks, the degree is kept at two.

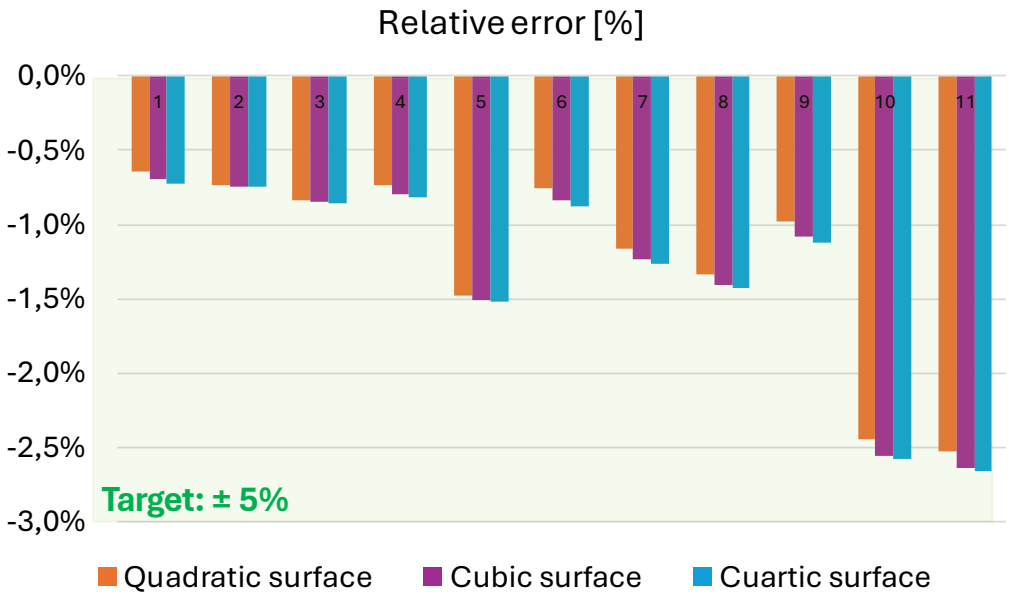

Figure 4: Relative comparison of the frequencies of the first nine modes for different IGA degrees.

To finalize the plate benchmark analysis, the shape of mode 8 for the three models is shown in *Figure 5*. The same shape can be observed in all cases. The time duration for the plate is the same between FEA and IGA, but it may not be representative of more complex models.

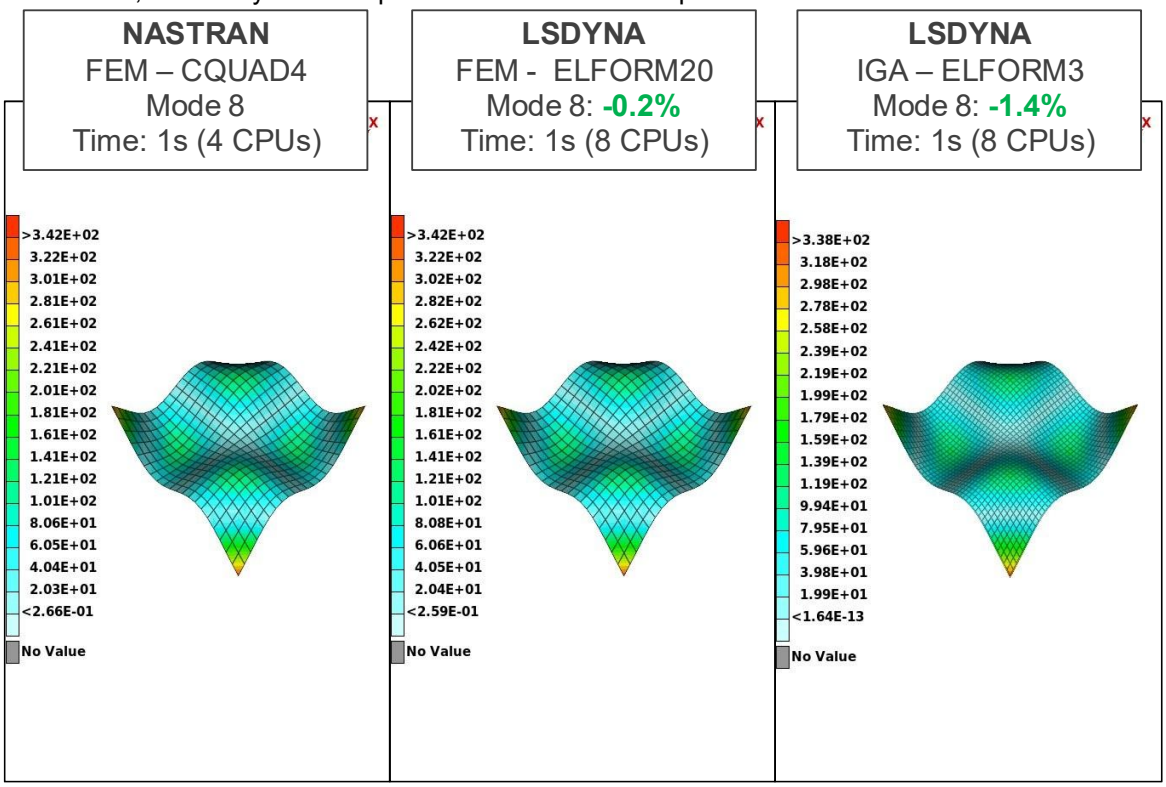

Figure 5: Shape of the mode 8 with the field of the strain energy. At the left the NASTRAN model, at the middle the FEA LS-DYNA model and at the right the IGA LS-DYNA model.

3.2 B-pillar benchmark

This second benchmark uses the B-Pillar of the Formentor to represent an intermediate step between elemental geometries and complete vehicle structures. This benchmark will also allow to confirm that using the ACM2 spotweld configuration in LS-DYNA works and the results are similar to the original CWELD configuration in NASTRAN. The B-Pillar is selected because of its structural significance in vehicle design and its moderate geometric complexity. The top and bottom of the B-Pillar are fixed to perform the modal analysis. The material properties used are the same as the plate benchmark for the structural material and for the spotwelds a material with a Young's Modulus of $E = 20000\,MPa$, a Poisson's ratio of $\nu = 0.3$, and a density of $\rho = 7.85E-9\frac{T}{mm^3}$ is used. *Figure 6* shows an exploded view of the parts that make up the B-Pillar. Each of the parts is connected to the others using CWELDs in the original model, and for LS-DYNA are transformed to hexahedral elements with the spotweld material assigned. The same image shows the results for mode 5 between the original NASTRAN-FEA model and the LS-DYNA-FEA model. The strain energy density is scaled in the LS-DYNA model to make the pattern match the NASTRAN pattern, as LS-DYNA calculates the strain energy density differently from NASTRAN. But it shows good agreement between both models. The stiffer response in the ACM2 spotweld configuration is expected, as the modification now takes more area connected with the ties to the hexahedral elements compared to the original CWELD connection. But this increase, being small is tolerable.

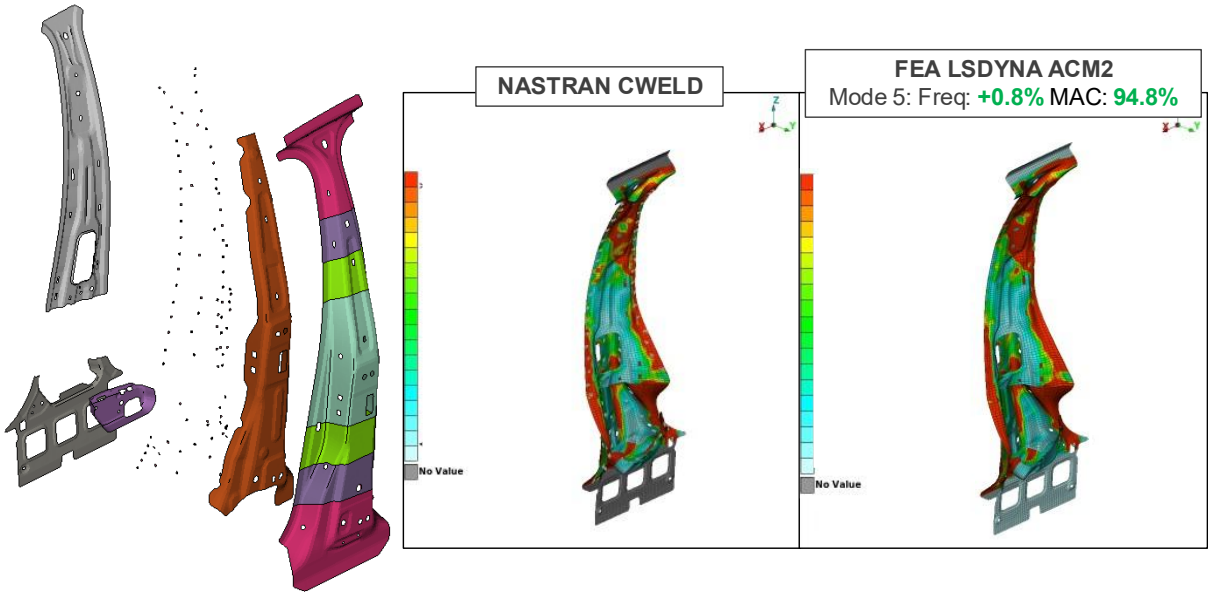

Figure 6: At the left side the exploded view of the Formentor B-Pillar and at the right side the strain energy density of the mode 5 of the B-Pillar for the original NASTRAN model and for the FEA LS-DYNA version.

Figure 7 shows the results of the MAC comparison for the low range frequencies of the B-Pillar between the original NASTRAN model using CWELD for the spotweld configuration and the LS-DYNA IGA model using the ACM2 configuration for the spotwelds. The overall results for the first eight modes are good and closer to the industry standards, but starting with the 9th mode, the differences are significant and not presented. This mode is also the beginning of the medium frequencies, therefore not interesting for this initial assessment, which is on low frequencies. For medium and high frequencies, it would be better to compare IGA results to experimental results and not directly with NASTRAN results, as finite elements are known to not capture medium and high frequencies well. But the use of the ACM2 spotwelds configuration is deemed correct and can be used for the next benchmark.

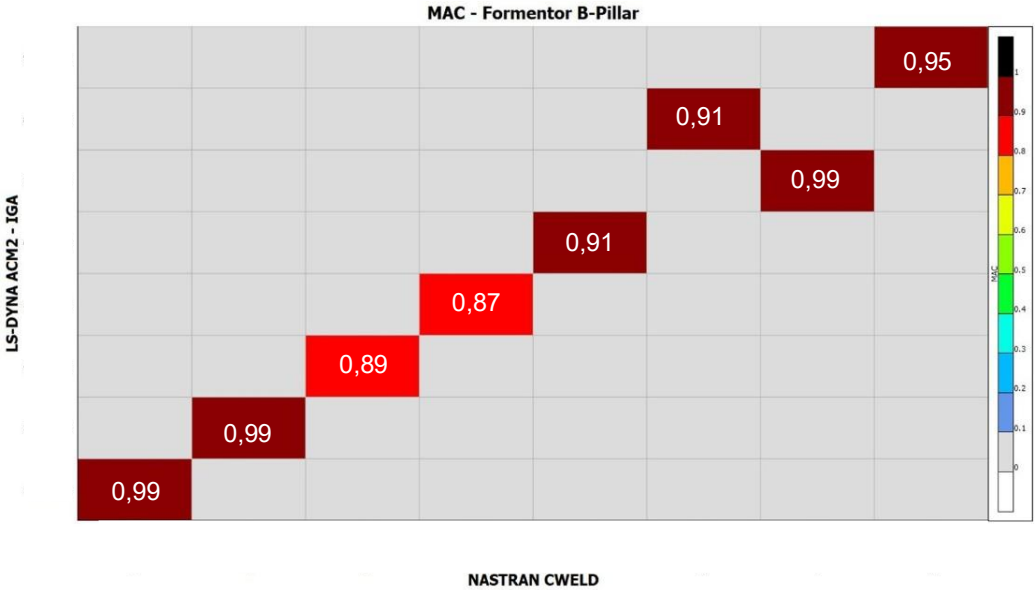

Figure 7: MAC comparison between the IGA B-Pillar model and the original NASTRAN model

3.3 BiW benchmark

The last benchmark for IGA shells is done using the BiW model of the Formentor to represent the production-level analysis challenges. To ensure a fair IGA comparison to FEA first the NASTRAN model with spotwelds in the ACM2 configuration and the LS-DYNA FEA models are compared to ensure that the change in the spotweld configuration does not introduce noise in the results and is consistent with the previous benchmark results. The conditions for the BiW are free-free. *Figure 8* shows the frequency

comparisons of the modes between the NASTRAN original model with CWELDs, the modified NASTRAN BiW model with ACM2 and the ACM2 LSDYNA model using FEA. As expected, the NASTRAN model using the ACM2 spotweld configuration shows a stiffer response. The LS-DYNA results show lower frequencies, in accordance with the plate and B-pillar results. The overall relative error is almost inferior to 0.5% compared to the original NASTRAN model. To give some perspective, the measurement tools for vibration experiments have an approximate tolerance of 1 Hz, which for the first modes of the BiW structure is much more than the error obtained with the spotweld configuration change. The figure also shows the shape at maximum deformation for the torsion mode of the BiW structure.

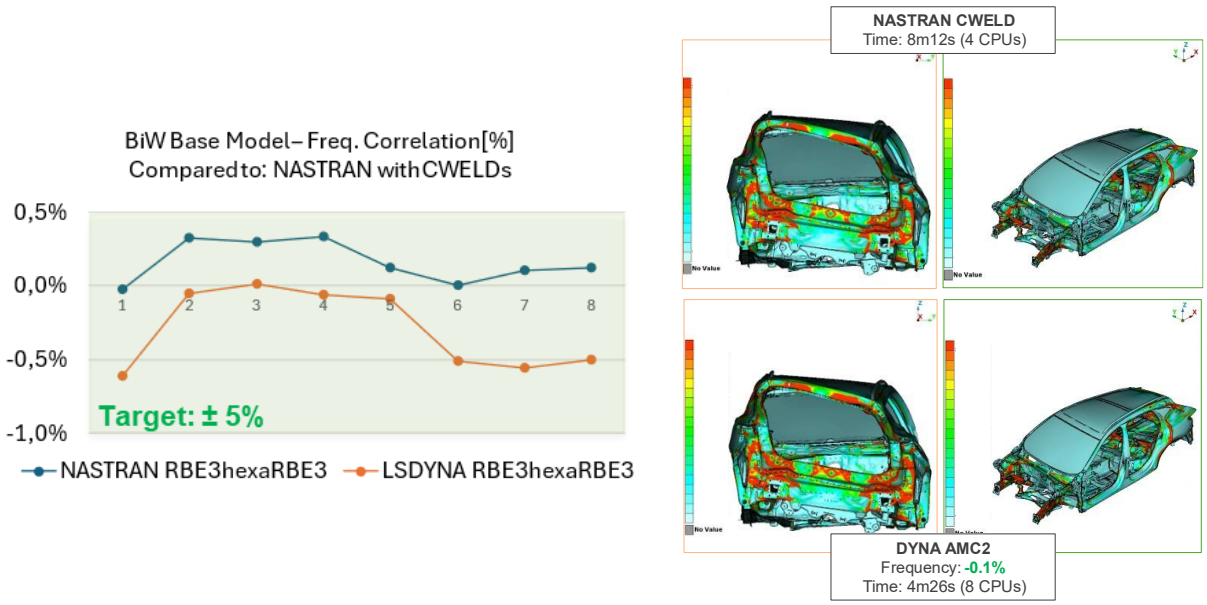

Figure 8: Relative comparison of the frequencies of the first eight modes (without considering the 6 initial rigid body modes) of the BiW of the Formentor changing the spotweld definition from CWELD to a ACM2 configuration. At the top right side the shape deformation for the torsion mode (mode 2) of the original NASTRAN model and at the right bottom side the same mode for the LS-DYNA model with the ACM2 configuration for the spotwelds.

Confirmed that the change in the spotweld configuration does not affect the results, two scenarios are considered for the introduction of IGA to the BiW model. The first scenario is to substitute the rear ring parts, composed of 5 different parts. For each part the IGA model is created from the original CAD geometry and the FEA meshes are swapped. The connections to the rest of the structure and between parts remain the same. The rear ring is an important region of the structure for the NVH team, as it is where they have more freedom to propose countermeasures to the structure compared to other parts of the vehicle. This scenario allows to see the effect of the IGA parts in a global mode of the vehicle. The second scenario substitutes the crossbeam in the front bumper region, the Crash Management System (CMS) traverse. Its a single large component in the frontal region. This will allow to see the local influence of the IGA part, as there is a mode with a significant influence from this component. *Figure 9* shows an exploded view of the parts to be swapped by IGA in the two scenarios.

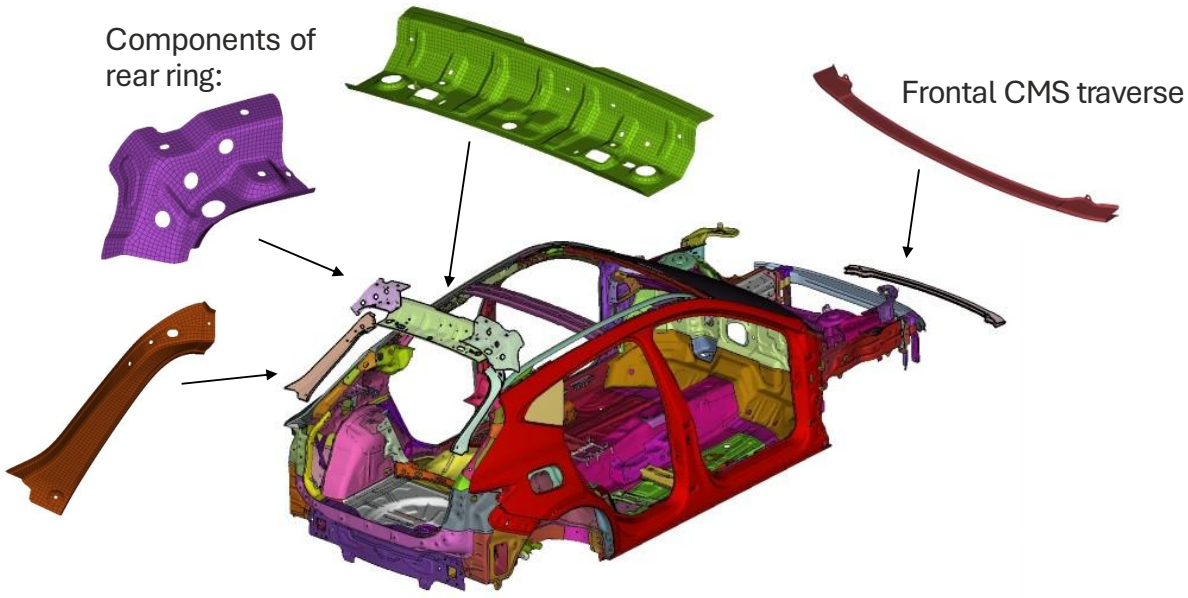

Figure 9: Exploded view of the BiW with the components of the two scenarios considered highlighted.

The original SEAT model has an element size for FEA of 8mm, a standard size in the industry. The parts of the rear ring are created with knot spans of 8mm. However, for the CMS traverse, the mesh is reduced to 2mm. In next Section 5.1 Geometry creation there is an explanation of why no larger knot spans were used for this component, as it is related to a current technical constraint. *Figure 10* shows the result of the MAC comparison for the first 8 non-rigid body modes (there is 6 rigid body modes) of the BiW between the original NASTRAN model and the LS-DYNA model with the rear ring modeled with IGA. All modes show a good correlation under industrial standards, with mode 13 being the one with higher difference. The shape of mode 8 is shown with the energy strain density plotted. Mode 8 is the one where the rear ring have more importance. Again, the normalization that LS-DYNA does of the strain energy density shows a different pattern, but the frequency and the mode shapes are correct. Both models (FEA and IGA) have an average element size of 8mm.

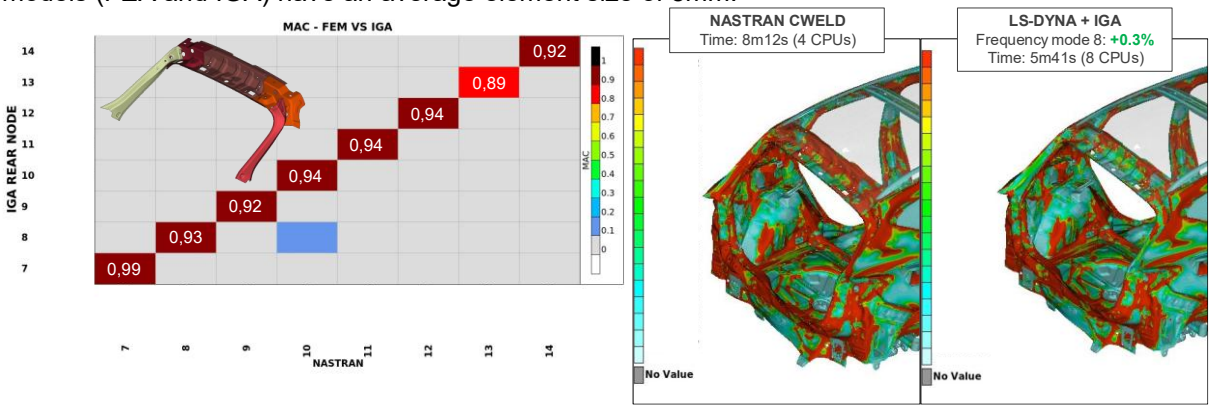

Figure 10: MAC comparison between the original NASTRAN Formentor model and the LSDYNA hybrid model with the rear ring components swapped for IGA discretizations. At the left side the MAC table starting at the non rigid body modes and at the right side the shape of mode 8 with the strain energy density field plotted.

Figure 11 shows the results of the MAC comparison for the first 8 non-rigid body modes of the BiW between the original NASTRAN model and the LS-DYNA model with the CMS traverse modeled with IGA. The first mode after the rigid body modes, mode 7, affects mainly the CMS component itself. For this mode the MAC correlation is of 0.99 showing almost a perfect matching shape between the NASTRAN model and IGA model. The rest of the modes also have good correlation values. The frequency difference for this mode is very similar to that of the NASTRAN model, showing an overall very good correlation. Again, in the strain energy density for the IGA models we cannot compare the scales due to a different normalization between LS-DYNA and NASTRAN. More on the strain energy difference is commented in Section 5.2 Strain energy density.

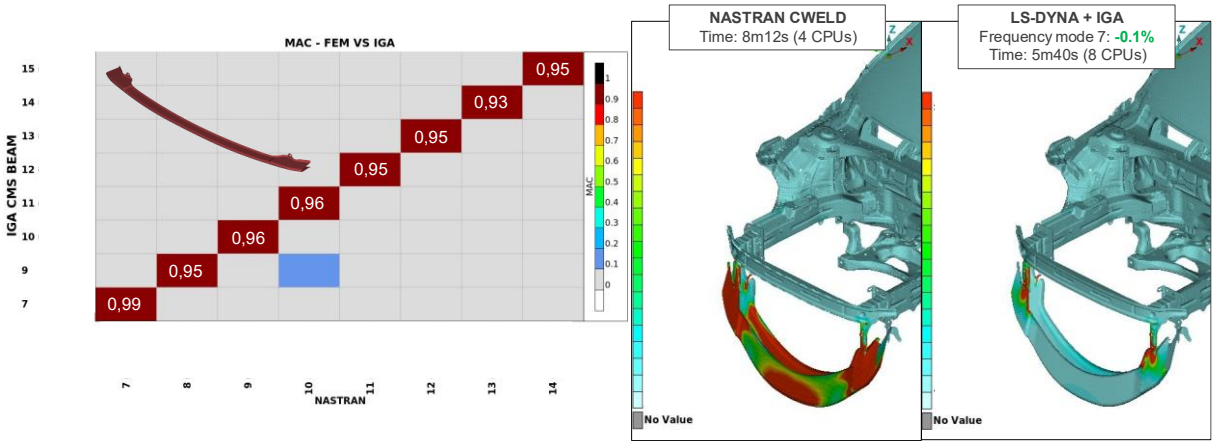

Figure 11: MAC comparison between the original NASTRAN Formentor model and the LSDYNA hybrid model with the CMS component swapped for IGA discretization. At the left side the MAC table starting at the non rigid body modes and at the right side the shape of mode 7 with the strain energy density field plotted.

4 IGA solid modal analysis assessment

For IGA solids three benchmark problems analysed are: the same square plate as in the shell case, one component of the Cardan joint of the Formentor vehicle, and the BiW also of the Formentor with the IGA Cardan model integrated. This study aims to be an initial rough assessment of the IGA solid elements readiness for NVH application.

The LS-DYNA implementation of trimmed IGA solid elements from [13], following the temporary workflow using the **`*IGA_DEV_VOLUME_XYZ`** is followed for all this benchmarks. This approach is necessary until the definitive *IGA keywords are available. This approach needs a solid part that is represented via a tetrahedral mesh. Some of the benchmarks are done using an existing FEA mesh and others using the new ANSA capabilities from last version 2025.1 to generate the IGA solid inputs for LS-DYNA starting from a CAD model (ANSA itself generates the FEA mesh).

4.1 Plate benchmark

The square plate model from Section 3.1 was re-evaluated using trimmed IGA solids approach to establish a baseline for IGA solid element performance. The same geometry, material properties and boundary conditions are used. A four-way comparison was conducted between the original NASTRAN shell element model (reference), a traditional FEA solid discretization performed with NASTRAN and LS-DYNA solvers using tetrahedral elements (and element types from *Table 1*), a trimmed IGA solid representation using the FEA tetrahedral mesh and a trimmed IGA solid representation created using ANSA and its new features from version 2025.1 that is able to generate the inputs for LS-DYNA from the CAD model (ANSA automatically generates the FEA mesh needed). The IGA models have a knot span of 2mm.

Figure 12 shows a comparison of the frequency values for the first 6 modes of the plate. The FEA results for both solid models (NASTRAN and LS-DYNA) show an almost exact response with a difference overall lower than 1% relative error compared to the NASTRAN shell results. The IGA results show a higher difference, but below the 5%, that can be considered acceptable. The results for the solid plate benchmark confirm that IGA solid elements exhibit a similar pattern to their shell counterparts, showing a less stiff response compared to the FEA discretizations.

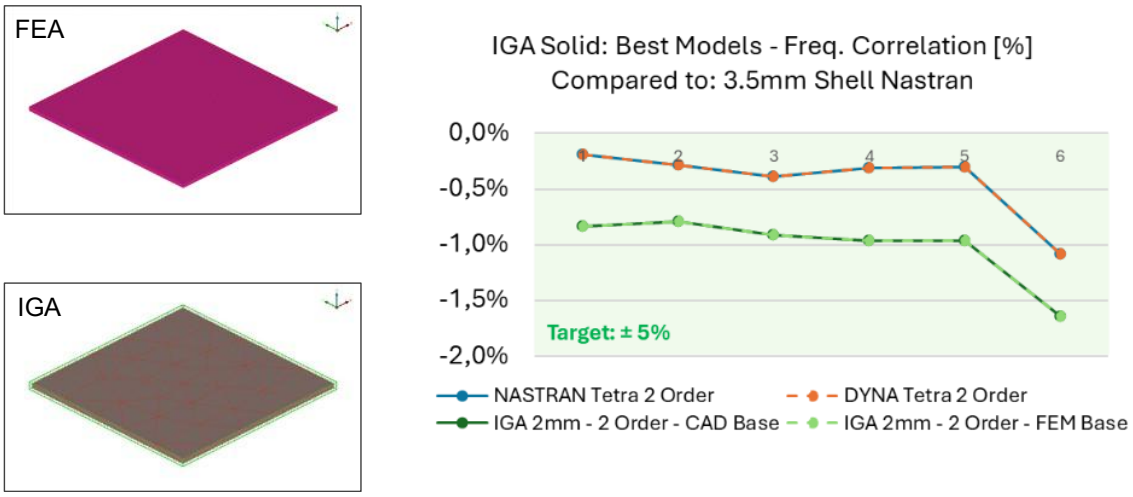

Figure 12: Relative comparison of the frequencies of the first six modes of the plates between the original NASTRAN-FEA shell simulation compared to the NASTRAN-FEA solid simulation, the LS-DYNA-FEA solid simulation and the LS-DYNA-IGA solid simulation.

Figure 13 shows a sensitivity analysis conducted to evaluate the effect of discretization size on the IGA solid model performance. Three different knot span configurations were tested: 2mm, 3.5mm, and 5mm. The variation in frequencies across different knot span sizes remained minimal for this simple geometry. However, it should be noted that this elementary benchmark may not provide definitive conclusions regarding mesh sensitivity for more complex geometries.

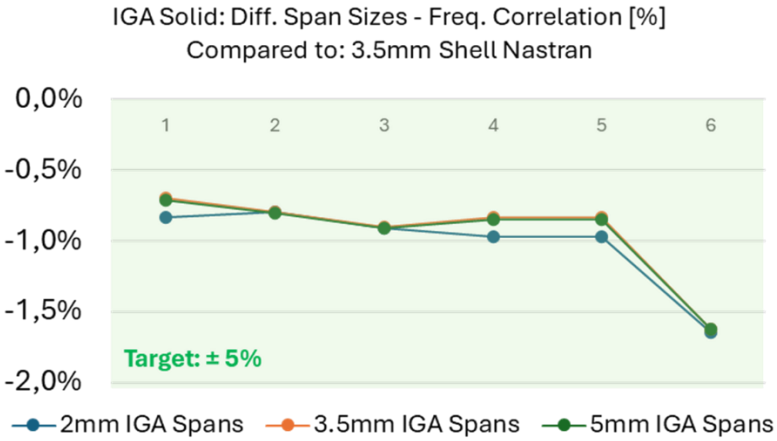

Figure 13: Relative comparison of the frequencies of the first six modes for different refinements of the IGA solid elements compared to the NASTRAN shell solution.

4.2 Simple component benchmark (Cardan joint)

A Cardan joint from the Formentor vehicle was selected as a representative solid component with moderate geometric complexity. The original FEA model utilized a tetrahedral mesh with an average element size of 5mm. The IGA solid model was generated using a template provided by Dynamore, which creates an IGA box where the Cardan geometry is immersed. This approach represents a typical workflow for converting existing CAD geometries to IGA solid representations. Three models are compared: the original NASTRAN FEA tetrahedral model (reference), the LS-DYNA FEA tetrahedral model and the LS-DYNA trimmed IGA solid model. The IGA solid was generated with an extended configuration and degree 2. *Figure 14* shows the results of the modal analysis of the Cardan joint. The results show consistent behaviour with the previous benchmark. Again, the IGA solid model exhibited lower natural frequencies compared to both FEA implementations, indicating a less stiff response.

Figure 14: Relative comparison of the frequencies of the first nine modes of the Cardan joint between the original NASTRAN-SOLID shell simulation compared to the LSDYNA-FEA solid simulation and the LSDYNA-IGA solid simulation.

Figure 15 shows the results of the MAC comparison for the first 9 non-rigid body modes of the Cardan joint between the original NASTRAN model and the LS-DYNA IGA model solid model. The overall results for the first six modes are identical but starting with the 7th mode the differences increase. It is worth noting that strain energy density plots could not be generated in the META post-processor in some cases. However, when the analysis has only IGA solids generated by Dyna's Template, it is possible to plot the strain energies.

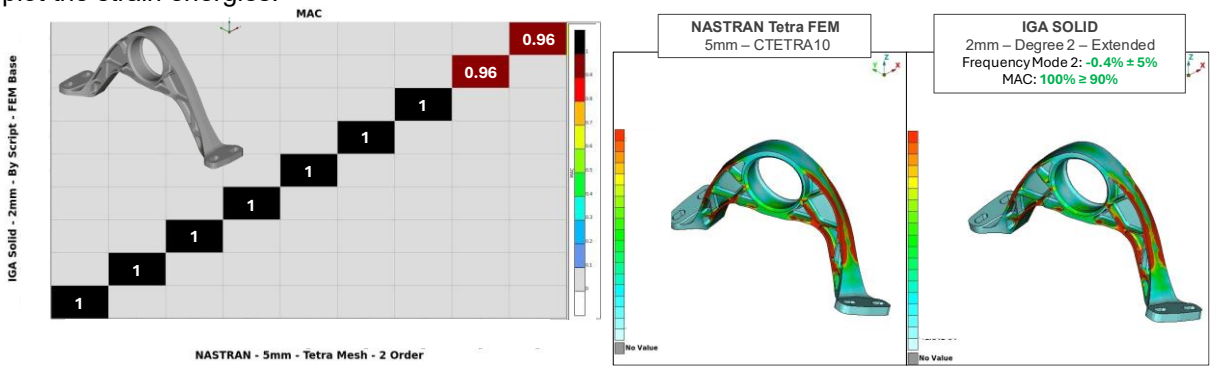

Figure 15: MAC comparison between the original NASTRAN Formentor solid model and the LSDYNA trimmed IGA solid model.

4.3 BiW benchmark

For the final benchmark, the Cardan joint IGA solid model developed in Section 4.2 was integrated into the full BiW structure of the Formentor vehicle. This hybrid modeling approach allows for the assessment of IGA solid elements within a complex structural assembly, representing realistic automotive applications. The baseline model utilized the same BiW structure as in Section 3.3, with the original FEA Cardan joint replaced by its IGA solid counterpart. The connection between the IGA solid component and the surrounding FEA structure was established attaching a **`*CONSTRAINED_NODAL_RIGID_BODY`** (*CNRB) of duplicate nodes of the interpolation mesh to the Cardan joint via a **`*CONTACT_TIED_NODES_TO_SURFACE_OFFSET`** as recommended by the temporary workflow with

tetmesh input from LS-DYNA. *Figure 16* shows the Cardan IGA solid discretization integrated into the BiW structure of the Formentor.

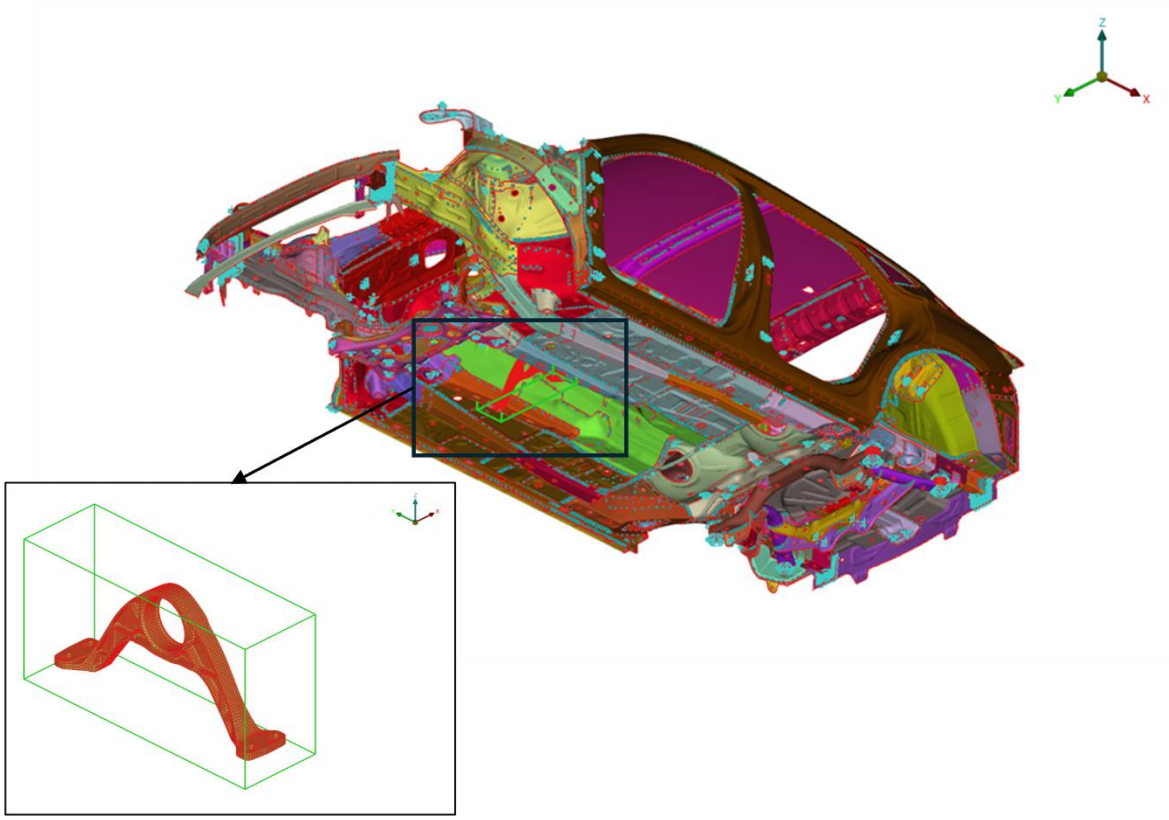

Figure 16: BiW trimmed IGA solid model integration of the Cardan joint in the Formentor vehicle.

The modal analysis results for the BiW with integrated IGA Cardan joint demonstrate the feasibility of incorporating IGA solid elements within a predominantly FEA structural model. *Figure 17* shows the results of the MAC comparison for the first 8 non-rigid body modes of the BiW between the original NASTRAN model and the LS-DYNA model with the Cardan joint modelled using trimmed IGA solids. The MAC correlation matrix shows acceptable agreement between the hybrid IGA-FEA model and the reference full-FEA model. The main reason for the differences in the MAC is the model translation to LS-DYNA; the Cardan IGA solid itself did not undergo significant changes in this respect. Due to the strain energy bugs mentioned before, it was necessary to plot the energy of the model as Von Misses tensions. This procedure is not ideal, but it is sufficient to examine the patterns of the results.

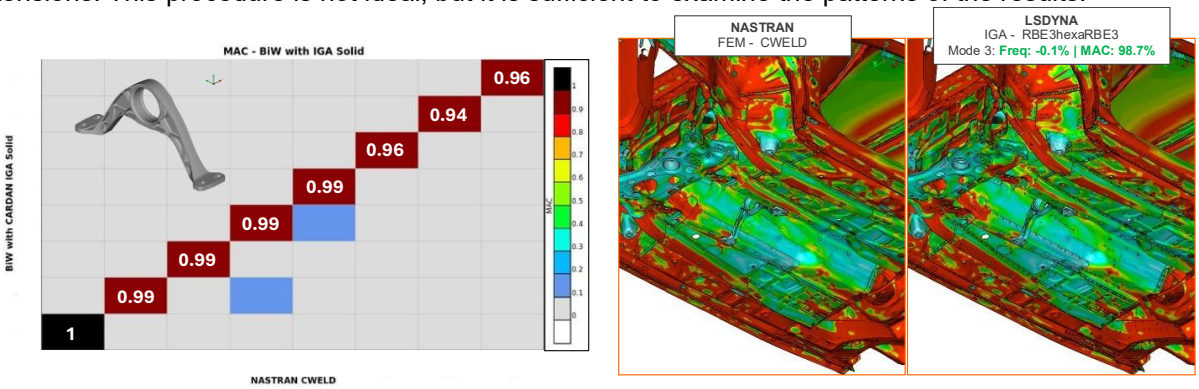

Figure 17: MAC comparison between the original NASTRAN Formentor model and the LSDYNA hybrid model with the Cardan joint component swapped for a trimmed IGA solid discretization. At the left side the MAC table starting at the non rigid body modes and at the right side the shape of mode 2 at the non rigid body modes with the Von Misses density field plotted.

5 Ongoing challenges

Given that the current IGA implementation in LS-DYNA has been tested mainly for crash applications, it was expected to find issues when applying it to NVH, which use the implicit time integration scheme. The following section is a recollection of some of the current challenges found during this study, which will probably be solved gradually in the future.

5.1 Geometry creation

During the BiW assessment presented in Section 3.3, the CMS traverse IGA shell model was implemented with a 2mm knot span, rather than the 8mm span used for the surrounding FEA elements. Initial attempts to model the CMS traverse with 8mm knot spans (consistent with the FEA discretization) produced notably inaccurate results. This observation prompted further investigation into the underlying causes of this discrepancy. *Figure 18* shows the results for varying knot span size for the IGA shell mesh of the CMS component for a modal analysis of only this part. The ANSA assistant tools for IGA are used to plot the distortion measure from the original midsurface geometry and it can be seen how for 8mm knot span the results are high. The zoom of the radius regions of the CMS traverse shows that the radius geometry is not perfectly captured and also some undulations in the flat face. These distortions seem to be critical for the modal analysis results as they modify the geometry features itself and can be seen in the results that for low knot span sizes, these values are reduced considerably obtaining good correlation results compared to the NASTRAN solution.

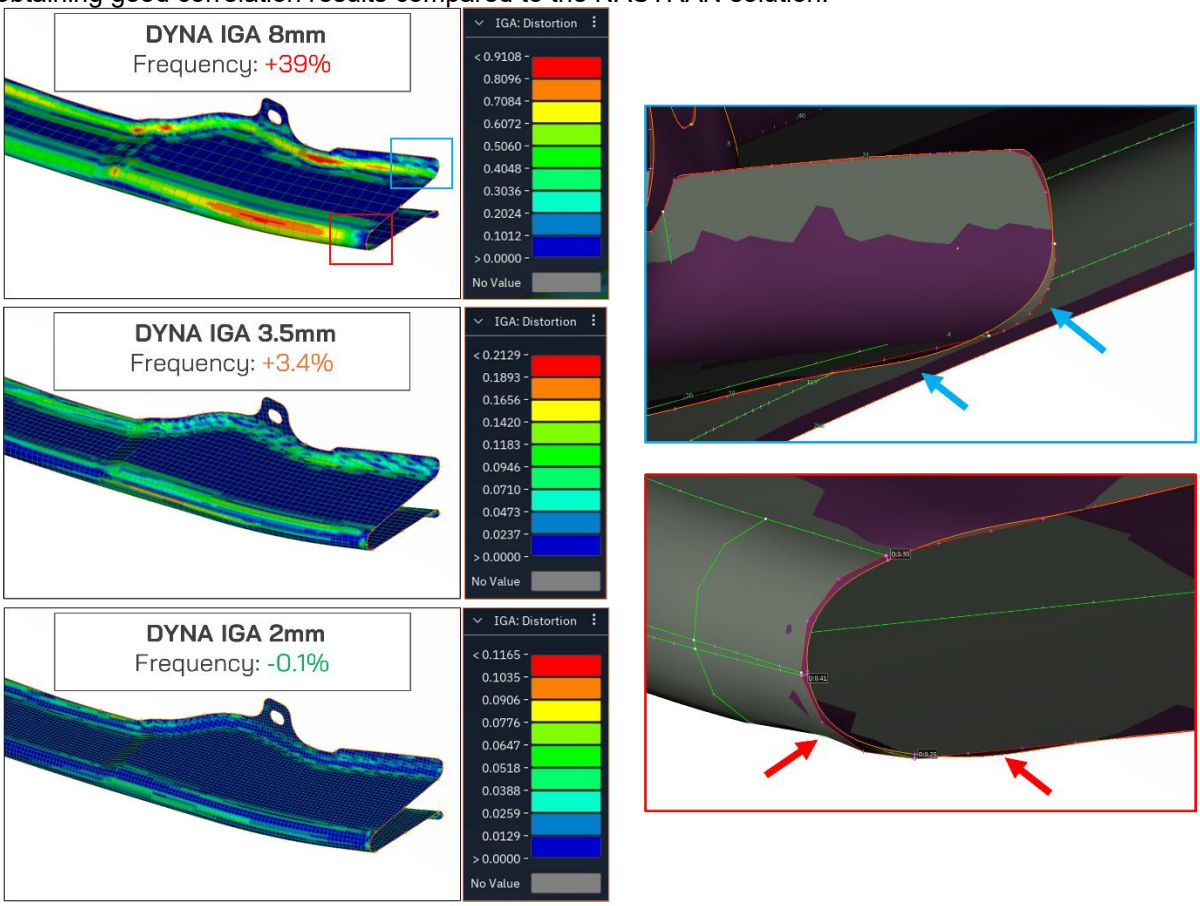

Figure 18: CMS results for varying knot spans. At the left side the distortion distribution calculated with the ANSA assistant for the 8mm (top), 3.5mm (middle) and 2mm (bottom) knot spans. At the right side a zoom at two areas of the 8mm knot span model where the IGA shell (orange border) has higher distortion compared to the original CAD surface and undulations on the flat plane can be observed.

To better understand and isolate the effect of geometric distortion, a simplified model was created by extracting a representative section of the CMS traverse. Three variant models were developed and compared: a single-patch IGA model with 8mm knot spans, a three IGA patches model with 8mm knot spans for each patch (flat face and radius) and a three IGA patches model with 8mm knot spans for flat regions and 3.5mm knot spans for curved patch. *Figure 19* shows the distortion results for each of the

cases described. The single patch suffers from undulations in the flat face and have high distortion in the radius region. The multi-patch approach with average knot span of 8mm avoid the undulations in the flat faces but the radius region still has high distortion. Finally, the multi-patch approach with refinement in the radius region captures well the geometry features. It is expected that improvements to the ANSA algorithm for geometry creation will improve or solve this problem. But the current user of IGA should be aware that for some coarse discretizations in IGA shells the geometry may have large enough distortions that affects the results.

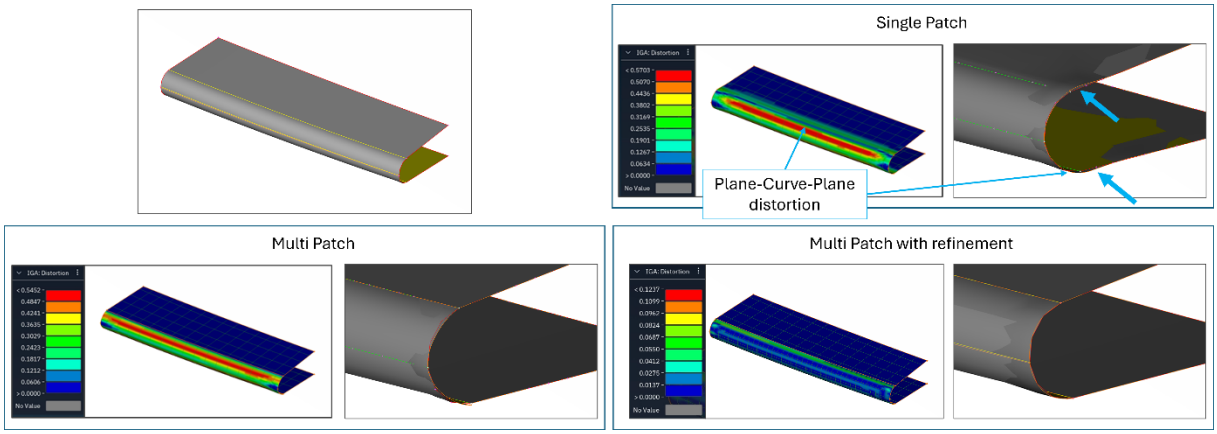

Figure 19: Multi-patch study in reduced model to identify multi-patch solutions that capture well geometry.

5.2 Strain energy density

The comparison of strain energy density patterns between NASTRAN and LS-DYNA revealed significant visualization differences, even when using identical FEA models. These differences stem from distinct normalization approaches employed by the two solvers rather than actual physical differences in the calculated results. When applying the same visualization scale, and trying to compare LS-DYNA and NASTRAN FEA results the patterns do not match. However, by changing the fringe scale of the LS-DYNA results, equivalent strain energy density patterns can be achieved for both models.

While the normalization issue can be addressed for FEA models with this workaround, additional complications arise when visualizing strain energy density for IGA models, particularly when multiple IGA shells are present. Small differences in average knot span sizes between IGA components affect the scaling of the strain energy density visualization, making it impossible to apply a uniform scale factor across the entire model. *Figure 20* illustrates this problem using two parts from the B-pillar model presented in Section 3.2. Despite being parts of the same structural assembly and with similar knot span average size, these components require different scaling factors in the fringe bar to achieve the same NASTRAN strain energy density visualization patterns. This makes impossible to visualize the whole B-pillar with a similar pattern for the IGA shell modelling.

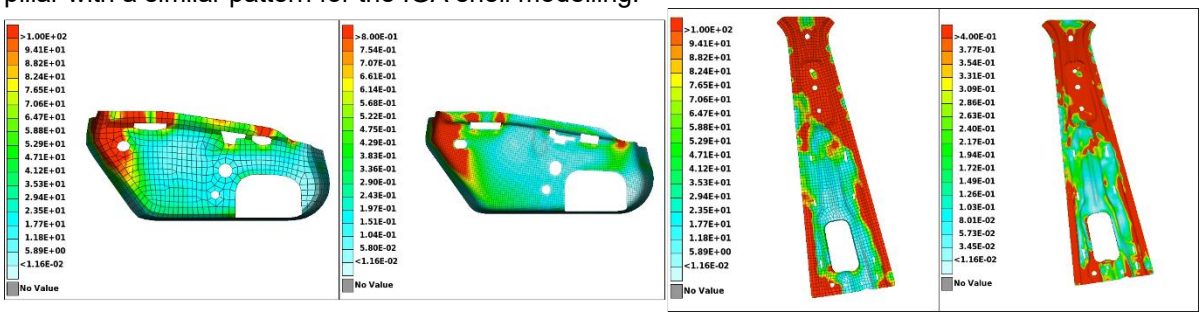

Figure 20: Scale comparisons for different parts on the B-Pillar of the Formentor using IGA shells.

For IGA solids, figure 21 shows that the strain energy visualisation currently does not work properly with them. A bug occurs at models generated by template and it is not possible to see the strain energy with hybrid models using FEM. For models generated using ANSA tools, it is not possible to visualise strain energy, even for IGA solid models alone. Strain energy patterns are essential for understanding structural behaviour, identifying critical regions and optimising designs. The challenge of visualising strain energy density represents a practical limitation for current NVH engineers when interpreting IGA results.

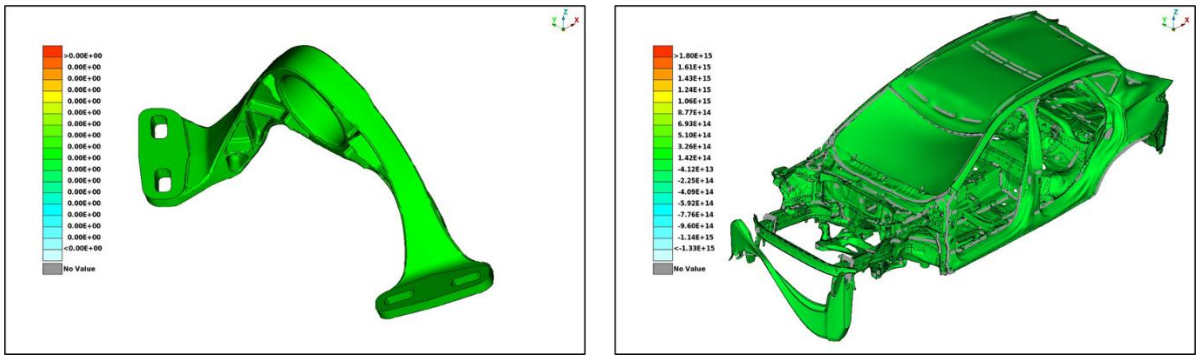

Figure 21: At left, the Scale's bug on Cardan modals when generated by ANSA and at right Cardan IGA solid generated with template and FEM associated with BiW of the Formentor.

5.3 Spurious modes

During the modal analysis of several IGA models, anomalous vibration modes were detected that had no physical counterpart in the corresponding FEA models. These spurious modes exhibited highly localized deformation patterns affecting small regions of the model, rather than the global deformation characteristics expected in valid structural modes. These anomalous modes primarily involved the movement of a limited number of control points, suggesting a numerical rather than physical origin. *Figure 21* shows an example of such a spurious mode, highlighting the localized nature of the deformation and its distinction from physically meaningful modes. The observed behaviour suggests that these spurious modes may be related to the stabilization mechanism for light control points for IGA. Further investigation needs to be done to clearly identify the source of this issue and if further actions needs to be done by the developers of LS-DYNA.

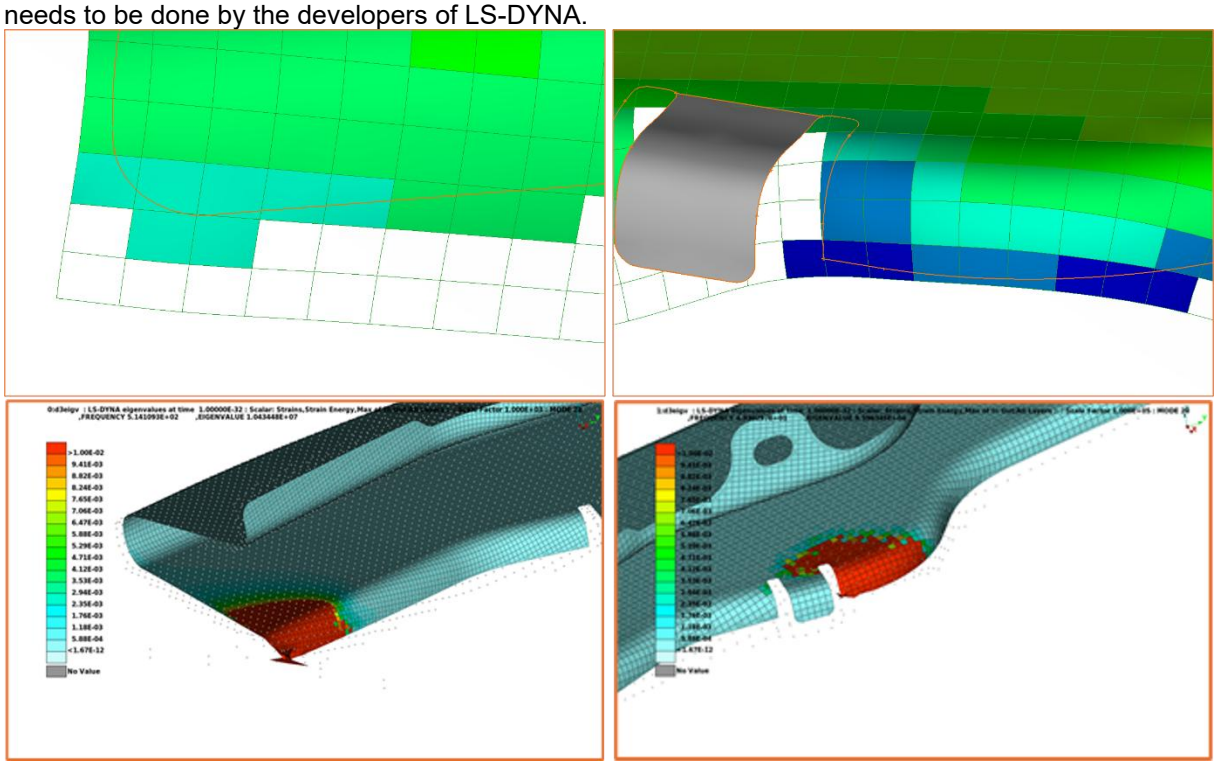

Figure 21: Spurious modes appearing in localized regions, probably due to light control points.

5.4 Cross-talk effect

Cross-Talk effect is an unwanted phenomenon that emerges when higher-order basis functions create artificial connections between physically disconnected regions in geometric models. It has already been reported in crash analysis [14-15] and a solution to it is already under investigation [16]. In implicit simulations it is also present as this is a phenomenon of trimmed IGA itself.

Figure 22 shows three different discretizations using trimmed IGA solids for the CMS traverse from Section 3.3 using different average knot spans. One region presenting Cross-Talk is highlighted for each of the models. The models are created using a FEA tetra mesh immersed in the IGA box. *Figure 23* shows the relative frequency of the modes of these three models compared to the NASTRAN FEA reference solution (shell model). It can be observed to have a higher stiffness in all cases compared to the NASTRAN reference solution. Coarser knot spans sizes produce a higher stiffness. These results are congruent with the Cross-Talk effect, as more regions get connected when using a coarser mesh. For 5mm knot spans, the modes change that much that some of the modes cannot be compared to the shape deformation of the original reference modes.

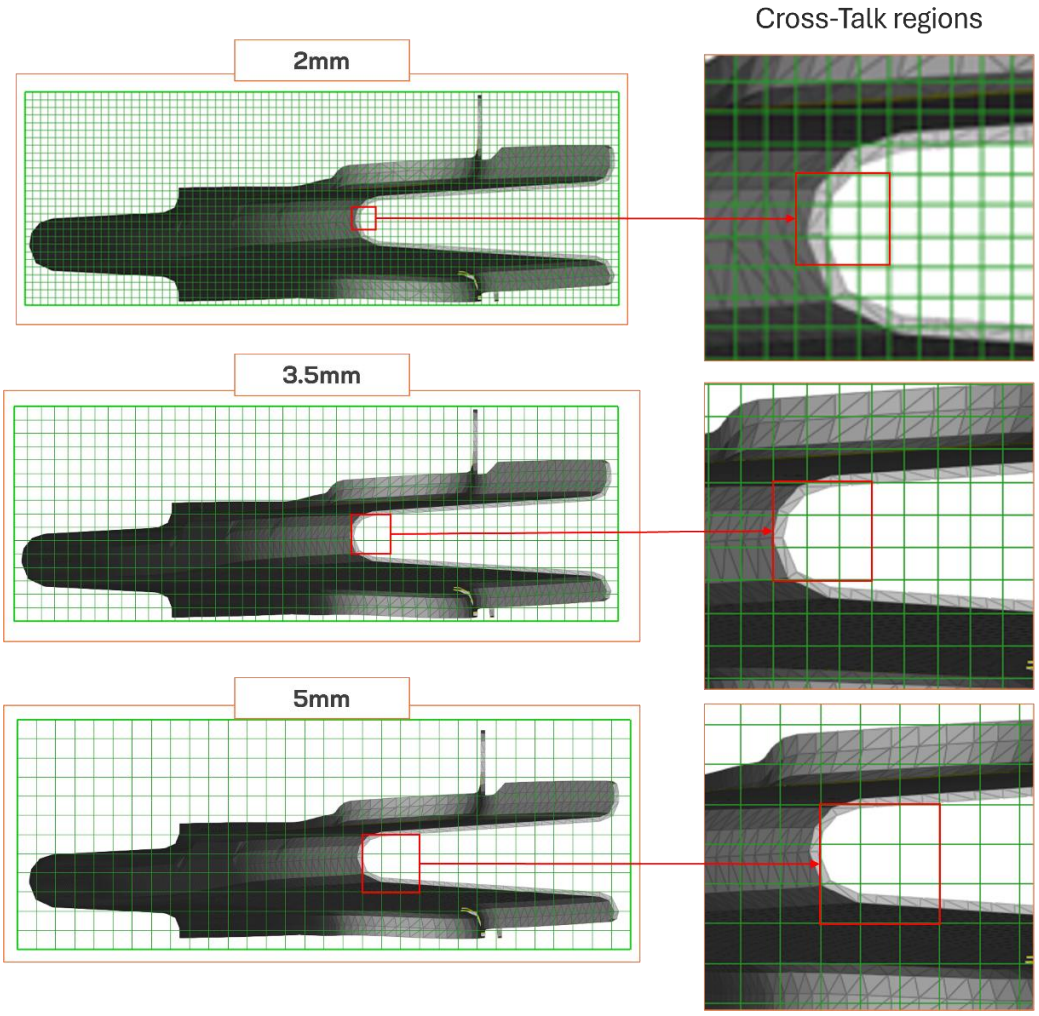

Figure 22: Cross-Talk regions in the CMS IGA solid model for different knot span sizes.

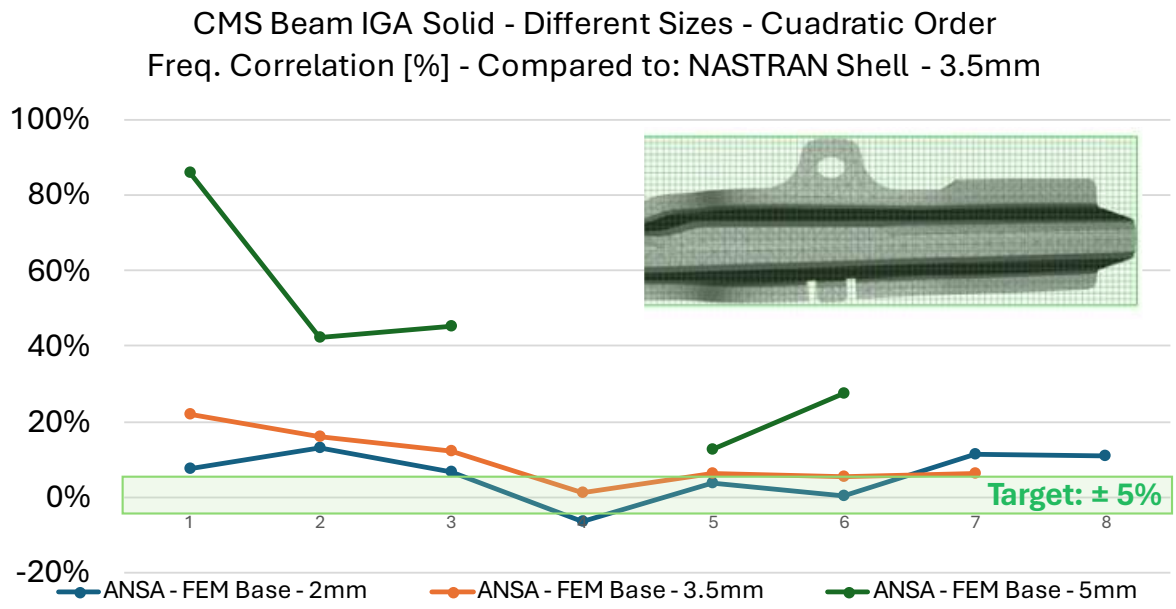

Figure 23: Comparison of frequency results given different knot spans with known Cross-Talk effect occurring

6 Conclusions and Outlook

Overall, as a first assessment of the IGA capabilities for NVH analysis using LS-DYNA, IGA shell and solid elements show good correlation with traditional FEA approaches, with frequency and MAC values deviations within acceptable tolerances. IGA consistently exhibits a less stiff response than FEA models across the benchmarks. Some first technical challenges have been reported in this initial assessment as geometry creation sensitivity, strain energy density visualization inconsistencies, spurious modes, and cross-talk effects. The current implementation is suitable for exploratory NVH analysis but requires additional refinement before production deployment. The status of the technology opens the door to more in depth analysis to explore IGA suitability for the medium frequency range where IGA have potential to give accurate results compared to FEA [4]. Future work will focus on modelling the whole BiW in IGA to explore ETS and FRF analysis and explore the use of IGA for initial NVH studies in production at the Feasibility phase of the project.

7 Literature

[1] Hughes T.J.R., Cottrell J.A., Bazilevs Y.: “Isogeometric analysis: CAD finite elements NURBS exact geometry and mesh refinement”, Computer Methods in Applied Mechanics and Engineering, Vol.194, 2005, p.4135-4195.

[2] Bauer, F., Yugeng, T., Leidinger, L., Hartmann, S.: "Experience with Crash Simulations Using an IGA Body in White", 14th European LS-DYNA Conference, 2023.

[3] Naito, T., Nishi, S., Ohya, T.: "Application of Trimmed Solid in Isogeometric Analysis to Aluminum Diecast Part”, 17th International LS-DYNA Conference, 2024.

[4] Cottrell, J.A., Reali, A., Bazilevs, Y., Hughes, T.J.R..: "Isogeometric analysis of structural vibrations”, Computer Methods in Applied Mechanics and engineering, Vol. 195, p. 5257-5296, 2006.

[5] M. Geradin and D.J. Rixen. “Mechanical vibrations: Theory and application to structural dynamics”. Wiley, 2015. ISBN 978-1-118-90020-8.

[6] Leidinger, L.: "Explicit Isogeometric B-Rep Analysis for Nonlinear Dynamic Crash Simulations: Integrating Design and Analysis by Means of Trimmed Multi-Patch Shell Structures”. PhD thesis, Technische Universität München, 2020.

[7] Altair help. “LS-DYNA to Nastran Conversion Mapping”. URL https://2022.help.altair.com/2022/hwdesktop/hm/topics/conversion_between_solvers/convert_ldsyna_to_nastran_mapping.htm

[8] Li, A.T., Cui, Z., Huang, Y. “LS-DYNA’s Linear Solver Development - Phase 1: Element Validation”. 15th International LS-DYNA Users Conference & Users Meeting, 2018.

[9] Li, A.T., Cui, Z., Huang, Y. “LS-DYNA’s Linear Solver Development - Phase 1: Element Validation Part II”. 15th International LS-DYNA Users Conference & Users Meeting, 2018.
[10] Predictive Engineering. “LS-DYNA Handbook for Structural Mechanics”. 2024. https://www.predictiveengineering.com/sites/default/files/LS-DYNA-Training/LS-DYNA-Handbook-2024.pdf
[11] Palmonella, M., Friswell, M.I., Mottershead, J.E., Lees, W. “Guidelines for the implementation of the CWELD and ACM2 spot weld models in structural dynamics”. Finite Elements in Analysis and Design, Vol. 41(2), p. 193–210, 2004.
[12] Hexagon. “MSC Nastran 2022.1 Quick Reference Guide”. URL https://documentation-be.hexagon.com/bundle/MSC_Nastran_2022.1_Quick_Reference_Guide/raw/resource/enus/MSC_Nastran_2022.1_Quick_Reference_Guide.pdf
[13] Hartmann, S., Leidinger, L., Bauer, F., Benson, D., Liping, L., Nagy, A., Nguyen, L., Pigazzini, M. "Updates on trimmed IGA B-Spline Solids”, 17th International LS-DYNA Conference, 2024.
[14] Cruz, P., Martorell, Ll., Ros, A., Dominguez, A.: "IGA technology validation for forefront crashworthiness CAE analysis”, 9th BEFORE REALITY Conference, 2023.
[15] Lian, Z., Leidinger, L., Hartmann, S., Bauer, F., Wüchner, R.: "Towards the Solution of Cross-Talk in Explicit Isogeometric B-Rep Analysis”, 14th European LS-DYNA Conference, 2023.
[16] Lian, Z., Leidinger, L., Hartmann, S., Bauer, F., Pabst, M., Krisadawat, C., Wüchner, R.: "Cross-talk effects in trimmed isogeometric shells and the control point duplication approach”, Computer Methods in Applied Mechanics and Engineering, Vol. 438, 2025.